

**Contrails: Observations, formation
mechanisms, atmospheric impacts,
uncertainties**

A contribution to the project:

**Identifying the uncertainties in radiative forcing of climate from
aviation contrails and aviation-induced cirrus**

by

UK Defence Evaluation and Research Agency (DERA)

in cooperation with

Hadley Centre for Climate Prediction and UK Meteorological Office

supported by

UK Gov. Department of the Environment, Transport and the Regions

PD Dr. Bernd Kärcher
German Aerospace Center (DLR)
Institute of Atmospheric Physics

March 29, 2000

Contents

1	Introduction	3
2	Thermodynamics of Contrail Formation	5
3	Precursors for Contrail Ice Particles	9
4	Conceptual Model of Contrail Formation	15
5	Contrail Properties and Freezing Mechanisms	19
6	Processing of Aerosols in Contrails	25
7	Impact of Aircraft Particulates on Cirrus	27
8	Impact of Aircraft Particulates on Chemistry	31
9	Uncertainties, Impacts, and Future Research	33
10	References	37

List of Figures

2.1	Atmospheric conditions supporting contrail formation	5
2.2	Contrail thermodynamics: A qualitative picture	6
2.3	Contrail thermodynamics: A quantitative picture	8
3.1	Aerosol processes in aircraft exhaust plumes and contrails	9
3.2	Size distributions of particles present in aircraft exhaust plumes	10
3.3	Exhaust soot and sulphate particles observed in an aircraft plume	11
3.4	Graphite surface covered by a liquid $\text{H}_2\text{SO}_4/\text{H}_2\text{O}$ droplet.	12
4.1	ATTAS contrails seen from the Falcon at 100 m distance	15
4.2	Contrail optical depths under threshold formation conditions	17
5.1	Size distribution of ice particles observed in a young contrail.	19
5.2	Soot-induced freezing pathway in aircraft contrails	21
5.3	Phase diagram of $\text{H}_2\text{SO}_4/\text{H}_2\text{O}$ droplets in an exhaust plume	23
6.1	Aerosols processed in an evaporating contrail	25
7.1	Contrail-to-cirrus transition: Observed particle spectra	28
7.2	Contrail-to-cirrus transition: Numerical simulation	30

Chapter 1

Introduction

Aviation emissions represent one particular source sector that may contribute to climate change. Climate change may arise from a number of chemical and cloud physical processes affecting radiative forcing. The Intergovernmental Panel on Climate Change (IPCC) assessment [IPCC, 1999] concluded that of the factors from aviation emissions that contribute to radiative forcing, probably those of contrails and potential increased cirrus cloudiness were the largest.

However, these factors – aviation particulates and their impact on aerosols and clouds – are among those with the largest uncertainty. In terms of reducing these uncertainties, contrails and contrail-induced cirrus represent a scientific research priority area.

The overall goal of the project as requested by DETR is to review the current understanding of the main causes of uncertainty in the climate effect of contrails. The goal of this contribution is to review the current knowledge – both from observations and theory – of contrail formation mechanisms, microphysical properties of contrails, potential atmospheric impacts, and major uncertainties in this area of research, in particular by addressing the following questions:

- How do contrails form from aerosols present in aircraft exhaust plumes ?
- How accurately can we predict contrail formation ?
- What are the uncertainties in mechanisms for contrail formation ?
- How could changes in engine emissions affect contrail formation ?
- How much is known about persistent contrails and cirrus resulting from aircraft particulates ?
- What are the potential chemical effects of aviation-produced aerosols and clouds in the atmosphere ?

This review is organised as follows. Chapter 2 describes the thermodynamic contrail formation conditions. Chapter 3 introduces the different aerosol types present in aircraft plumes that serve as precursors for the nucleation of ice particles in contrails. Chapter 4 presents an analytical, phenomenological model for contrail formation that predicts most of the general optical and microphysical features of contrail ice particles.

Chapter 5 reviews properties of young contrails from field observations and elucidates the current understanding of freezing mechanisms in nascent exhaust plumes. Chapter 6 explains how aerosols from the exhaust and the ambient atmosphere become altered in contrails in terms of size spectrum and chemical composition. Chapter 7 and Chapter 8 review the impact of aircraft particulates on chemistry and cirrus formation, including a discussion of the properties of long-lived contrails and their transition into cirrus clouds. Chapter 9 summarises uncertainties and open questions that have been addressed in the previous chapters and describes potential atmospheric impacts, pointing to future avenues of research in this field. Chapter 10 contains the list of references.

I thank David Lee, Bob Lunnon, John Tilston, Phil Clare, and Geoff Jenkins for the cooperation during this cross-disciplinary project. I acknowledge the fruitful discussions with Klaus Gierens, Susanne Marquart, Franz Schröder, and Ulrich Schumann from DLR during the preparation of this work.

Chapter 2

Thermodynamics of Contrail Formation

This chapter reviews how contrails form by considering basic thermodynamic principles. The thermodynamic approach does not require dynamical and microphysical details of contrail formation to be known. The underlying physical theory has been developed by Schmidt [1941] and Appleman [1953], and reviewed by Schumann [1996]. We briefly summarise how the threshold conditions – the atmospheric temperatures (T), pressures (p) and relative humidities (RH) at which contrails form – are derived. These conditions are summarised in Figure 2.1, together with the flight levels of subsonic and supersonic aircraft.

The formation of contrails is due to the increase in relative humidity that occurs during the mixing of the warm and moist exhaust gases emanating from the aircraft engines with the colder and less humid ambient air. A contrail will form when saturation with respect to liquid water is reached or surpassed in the plume.

The thermodynamic relation for contrail formation requires knowledge of the air pressure, temperature, and relative humidity at a given

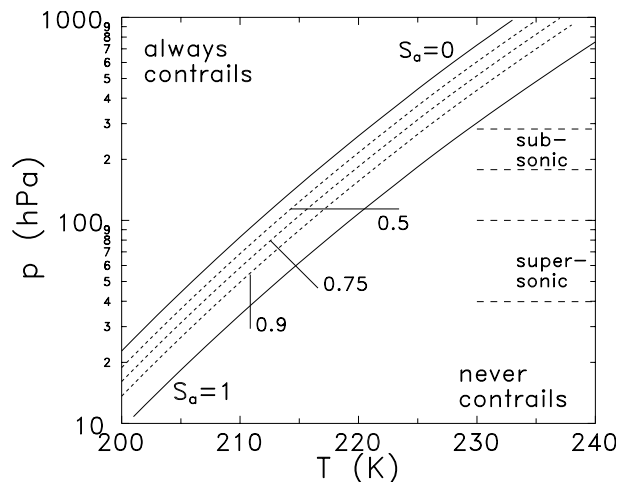


Figure 2.1: Diagonal curves represent the approximate critical pressure altitudes where contrails form at a given ambient temperature, parameterised by the ambient H_2O saturation ratio S_a . (S_a is equal to the relative humidity RH divided by 100%.) Subsonic and supersonic flight levels are indicated.

flight level, and fuel properties such as the emission index of H_2O , the combustion heat, and the overall aircraft propulsion efficiency. The thermodynamic criterion linking these parameters is well established and verified by in situ observations.

The thermodynamic relation for contrail formation is derived with the help of Figure 2.2. The saturation vapour pressure curves separate saturated (contrail-forming) from unsaturated (contrail-dissipating) regions. An air parcel starting at the exit plane of a jet engine (characterised by temperatures and water vapour concentrations well outside the graph) may pass point A of the mixing line during cooling and mixing. Typically, this happens within a few tenths of a second after the exhaust exited the engines.

The parcel then crosses the *liquid* saturation curve (solid line), where a contrail forms. The state of the atmosphere is represented by the point B, where the mixing line ends some time after emission. (Point B is reached asymptotically, provided the state of the atmosphere remains unchanged.) If the atmosphere at B is (super-)saturated with respect to ice, a persistent contrail may develop, otherwise the contrail starts evaporating when the mixing line again crosses the *ice* saturation curve.

The threshold conditions are derived with the help of the mixing line tangent to the liquid saturation curve in Figure 2.2. (Pressures are discussed in terms of mass mixing ratios and denoted by q_w for the following discussion.) Its slope at $T = T_+$ is denoted by $\sigma(T_+)$. A contrail forms whenever the condition

$$\frac{dq_{\text{sat}}}{dT} = \sigma(T) \leq \sigma(T_+) \quad (2.1)$$

is met, whereby $q_{\text{sat}}(T)$ is the liquid H_2O saturation mixing ratio. The upper (lower) black square in Figure 2.2, where the threshold relative humidity RH_{th} is 100 % (0 %), yields the maximum (minimum) threshold temperatures T_+ (T_-) for a contrail to form

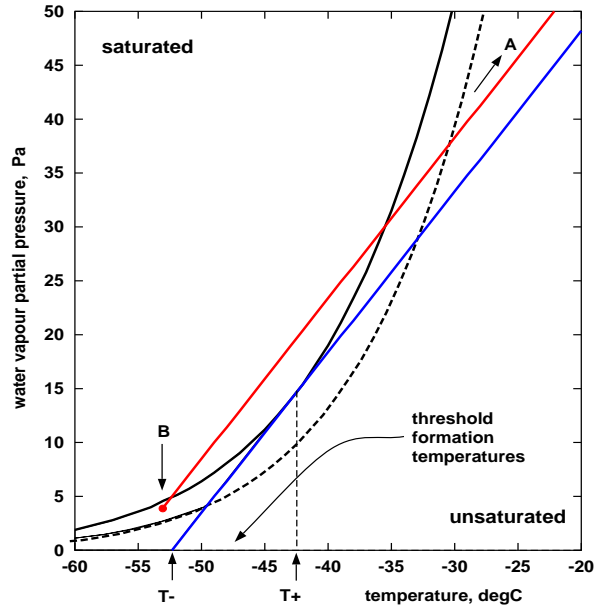


Figure 2.2: Schematic diagram of the H_2O saturation vapour pressures over liquid water (solid curve) and over ice (dashed curve) versus temperature. Line AB illustrates how an air parcel mixes isobarically in a jet plume, assuming that heat and water vapour mix similarly. Contrail age increases from A to B. The line tangent to the liquid saturation curve is used to derive the formation threshold temperatures, which lie between T_+ (water saturated air) and T_- (dry air). Figure courtesy of Klaus Gierens, with changes.

at a given pressure altitude p . Threshold temperatures $T_{\text{th}} \in \{T_-, T_+\}$ are uniquely related to corresponding relative humidities $\text{RH}_{\text{th}} \in \{0\%, 100\%\}$.

The T -derivative of q_{sat} in Eq. 2.1 is given by the Clausius-Clapeyron equation and reads

$$\sigma(T) = 0.622 \frac{L(T)}{RT^2} q_{\text{sat}}(T), \quad (2.2)$$

where L denotes the latent heat of evaporation and R is the specific gas constant for dry air. Along the mixing line, changes of the H_2O partial pressure q_w and the plume temperature combine such that

$$\sigma(T_+) = \frac{c_p \text{EI}}{Q(1-\epsilon)} \implies T_+, \quad (2.3)$$

[e.g., Schumann, 1996], where the specific heat capacity of dry air c_p , the emission index of H_2O EI, and the specific combustion heat of the jet fuel Q are well known quantities. The aircraft propulsion efficiency ϵ is defined as the fraction of combustion heat that is used up to propel the aircraft and thus is not available to heat the plume; it depends on Q , true air speed of the aircraft, the engine thrust, and fuel flow rate.

Equation 2.3 directly yields the maximum possible threshold formation temperature T_+ (corresponding to $\text{RH}_{\text{th}} = 100\%$) by iteration. The minimum threshold T_- (corresponding to $\text{RH}_{\text{th}} = 0\%$) simply follows by extrapolating the tangent mixing line to T_- , where $q_w = q_{\text{sat}} = 0$:

$$T_- = T_+ - q_{\text{sat}}(T_+)/\sigma(T_+). \quad (2.4)$$

The relative humidity is $\text{RH}/100\% = q/q_{\text{sat}}$. Combined with the equation for the tangent mixing line $q(T) = \sigma(T_+)(T - T_-)$, any pair of threshold conditions $\{T_{\text{th}}, \text{RH}_{\text{th}}\}$ can be calculated iteratively from

$$\frac{T_{\text{th}} - T_-}{T_+ - T_-} \cdot \frac{q_{\text{sat}}(T_+)}{q_{\text{sat}}(T_{\text{th}})} = \frac{\text{RH}_{\text{th}}}{100\%}, \quad (2.5)$$

where Eq. 2.4 has been inserted.

The derivation of Eq. 2.3 assumes that water vapour and heat mix similarly in the plume. For engines with a bypass this does not hold exactly, because the bypass air temperature is enhanced but does only contain H_2O at background concentrations. This additional, warm air causes a shift of the threshold temperatures calculated by Eq. 2.5 to slightly lower values. Values $\epsilon \simeq 0.3 - 0.4$ in Eq. 2.3 are typical for the present aircraft fleet. Increasing ϵ leads to contrail formation at higher ambient temperatures under otherwise unchanged conditions. Schumann [2000a] reports in-flight measurements that explicitly demonstrate the influence of ϵ on contrail formation. These observations show that an altitude range exists in which airplanes with high propulsion efficiency cause contrails while airplanes with lower ϵ cause none.

Figure 2.1 depicts the critical pressure altitudes p_{cr} for contrail formation versus background temperature as diagonal lines (using $\epsilon = 0$). These lines depend on the background relative humidity, expressed in terms of the saturation ratio $S_a = \text{RH}/100\%$. In the zone labelled ‘always contrails’, contrails will always form, regardless of the ambient humidity. In the region ‘never contrails’, contrail formation is very unlikely since supersaturations with respect to water are hardly ever observed in the atmosphere. In

the intermediate region, the formation of contrails, or their absence, depends on RH: the curves $p_{cr}(T)$ define the minimum value of RH at a given temperature and pressure.

It is interesting to note the changes of the threshold conditions caused by using fuel with different emission properties. For example, the use of liquid hydrogen (LH₂) for a future commercial aircraft fleet is currently under discussion. While kerosene is characterised by an EI of 1.26 kg H₂O per kg kerosene, LH₂-fuel emits 9 kg H₂O per kg LH₂ [Marquart, 1999]. Relative to kerosene, the ratio EI/Q entering Eq. 2.3 is about 2.55 times larger for liquid hydrogen fuel, because 0.357 kg of LH₂ contains the same energy available for combustion as 1 kg of kerosene.

Figure 2.3 shows that the high water vapour emissions from aircraft burning liquid hydrogen fuel increase the slope of the mixing line (compare the line labelled ‘kerosene’ with the line labelled ‘LH₂’). Consequently, less relative humidity is required to form contrails at a given temperature or contrails can form at higher temperatures at a given relative humidity. The highest formation temperature T_+ is about 10 K larger than in the case of kerosene.

These findings have important implications for the regions in the atmosphere which can be covered by contrails. For example, global model studies for commercial aircraft fleets as projected for the year 2015 show that the global mean, annually averaged contrail cover increases by a factor of 1.56 (ratio hydrogen-fuelled versus kerosene-fuelled planes), with the largest increases (factor 2) occurring in the tropics [Marquart, 2000].

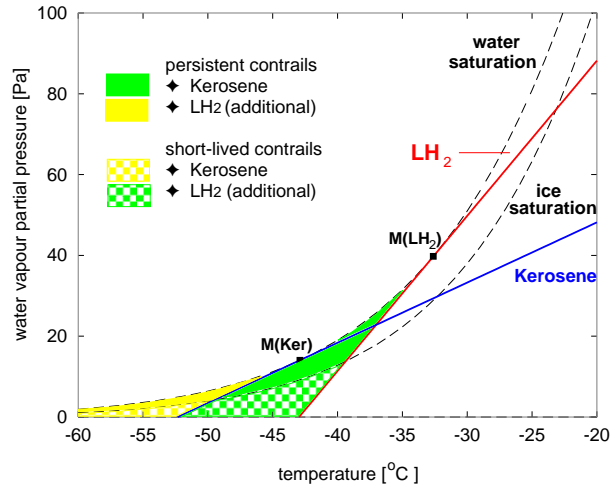


Figure 2.3: Diagram of the H₂O vapour pressures over liquid water and over ice (dashed curves labelled water saturation and ice saturation, respectively) versus temperature. The solid lines are calculated for mixing process using kerosene (lower line, LH₂) as jet fuel. The tangent points between the mixing lines and the liquid saturation curve are plotted as M(Ker) and M(LH₂). The shaded areas indicate the corresponding changes in the critical temperatures for persistent and short-lived contrails. Figure courtesy of Susanne Marquart, adapted from Marquart [1999].

Chapter 3

Precursors for Contrail Ice Particles

This chapter describes the particles produced within the jet engine combustors or formed within the fresh exhaust plumes under cruise conditions in terms of the size and chemical composition. Contrail ice particles predominantly form on these particles, although ambient aerosols entrained into the plume may in some cases also contribute to the particle budget in contrails.

The following aerosol types have been identified by in situ observations in aircraft exhaust plumes: (1) Liquid aerosols that consist of sulphuric acid (H_2SO_4), H_2O , and condensable organic species resulting from homogeneous nucleation. A fraction of these aerosols originates from chemi-ions (these are electrically charged

molecular clusters produced within the engine combustors). (2) Nonvolatile combustion aerosols that are mainly composed of black carbon soot, and to a lesser extent, of metallic particles. The soot particles very likely acquire a liquid surface coating in the

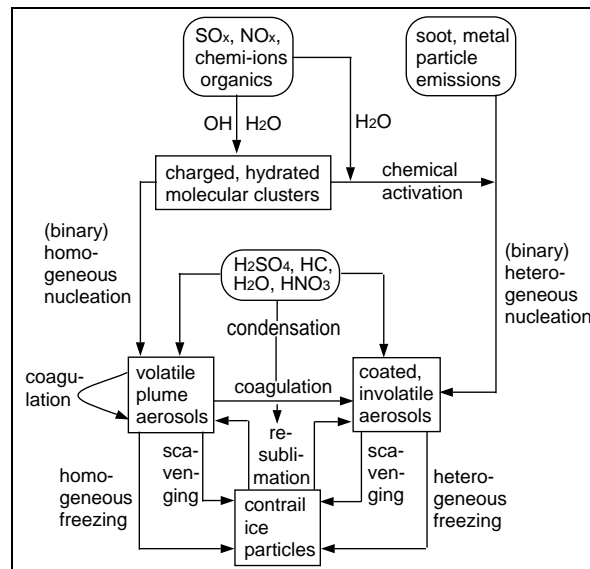


Figure 3.1: Schematic of aerosol dynamics and related chemistry in aircraft exhaust plumes and contrails. Round and rectangular boxes denote species emitted and formed in situ, respectively. The arrows and corresponding labels indicate transformation processes that are described by current numerical simulation models.

jet plume by interaction with sulphur (S) gases and $\text{H}_2\text{SO}_4/\text{H}_2\text{O}$ droplets. (3) Ice particles formed via freezing nucleation in contrails that rapidly take up the emitted H_2O in an initial growth stage. Figure 3.1 is a schematic of the physico-chemical processes that take place in aircraft plumes, involving these particle types [Kärcher, 1998a].

In what follows, several of the microphysical processes shown in this figure are discussed and the key characteristics of the different particle types present in exhaust plumes are described in more detail. Figure 3.2 is a schematic showing the size distributions of the different plume particle types at a plume age of 1 s as inferred from measurements and models. In the diameter range below 10 nm, the overall number size distribution is dominated by the volatile nucleation mode containing particles mainly composed of H_2SO_4 and H_2O (for fuel S contents above average values, which are of the order 0.4 g S/kg fuel).

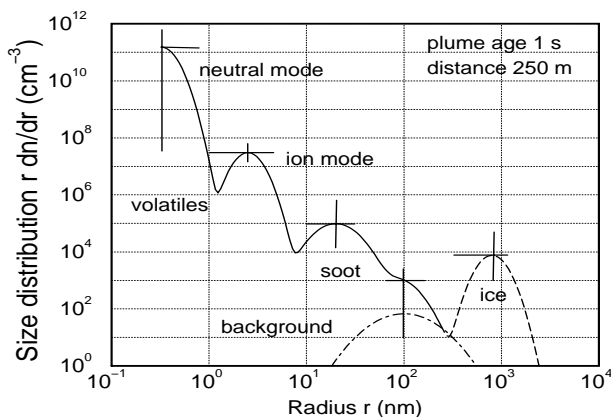


Figure 3.2: Size distributions of the particle types present in aircraft exhaust plumes. If a contrail forms, these spectra change (not shown) and ice particles are created (dashed curve). Bars denote variabilities of the respective parameters. A background spectrum (dot-dashed curve) is shown for comparison.

Model results suggest that the volatile particle size distribution may actually exhibit a bimodal structure [Yu and Turco, 1997]. Very recently, it became possible to directly measure the ultrafine particle size distribution above 3 nm diameter using a suite of condensation particle counters [Schröder et al., 1998, 2000a]. These measurements strongly support the following picture of new particle formation in young exhaust plumes, summarised in more detail by Yu et al. [1999].

The smaller particles are formed by aggregation of homogeneously nucleated clusters of hydrated H_2SO_4 molecules (neutral mode). The larger particles are formed by rapid scavenging of small molecular clusters by chemi-ions (ion mode). The growth of charged particles is preferred over the growth of neutral particles due to a net enhancement of the condensation and coagulation rates in a charged aerosol.

The concentration of cluster particles in the neutral mode depends strongly on the fuel S content. Their mean size is relatively invariant because of imperfect sticking of hydrated H_2SO_4 clusters after a collision. The mean size of the ion mode particles depends on the amount of material available for condensation. The concentration of the order 10^{17} ionised particles per kg fuel is relatively invariant, indicating that they form on virtually all of the emitted chemi-ions. Besides H_2SO_4 , which preferably condenses onto negative ions, organic exhaust species mainly condense onto positively charged clusters owing to their relatively large proton affinity. This implies that the ion mode actually consists of at least two modes (not resolved in Figure 3.2), and may contain exhaust hydrocarbons, besides H_2SO_4 and H_2O .

Aircraft jet engines directly emit solid soot particles. The term soot encompasses all primary, carbon-containing products from incomplete combustion processes. Besides the pure (optically black) carbon fraction, these products may also contain nonvolatile (gray) organic compounds. Exhaust soot is important in providing nuclei for liquid drop or ice crystal formation; soot strongly absorbs radiation and potentially affects air composition.

Soot emissions depend on engine types, power settings, flight levels, and possibly on the state of engine maintenance. The recent IPCC report [1999] gives a mean average soot emission index of 0.04 g soot per kg fuel for the present subsonic fleet. Older jet engines emitted up to 1 g/kg. No significant dependence exists between soot emission index and fuel S content. Electron microscope photographs of soot from in situ measurements reveal the irregular structure of the larger soot particles (agglomerates).

Petzold et al. [1999] have recently compiled size distributions, microphysical and optical properties, and emission indices of soot particles measured behind different jet engines. The results seem to support the presence of two soot modes (as those indicated in Figure 3.2), a primary mode with a mean diameter of 30 nm and a mode of agglomerated primary soot particles at 150 nm, with at least two orders of magnitudes differences in number concentrations. The fine black carbon particles dominate the light extinction of the plume aerosol.

Field data indicate, at least for the aircraft types considered, that modern engines emit less soot particles by mass and number, and that the particles are somewhat smaller than those from old-technology engines. There exist interesting similarities to soot/sulfate particle emissions from motorcars [Kittelson, 1998].

Soot particles fresh from jet engines very likely become hydrophilic due to activation by deposition of H_2O molecules and water-soluble species present in the exhaust, starting in the jet regime and perhaps even within the engines [Kärcher, 1998b]. Irregular surface features can increase the adsorptivity and amplify nucleation processes. It is known that soot hydrates more effectively with increasing fuel S content [Hagen et al., 1992]. For average and high sulphur levels, H_2SO_4 is likely the primary soluble constituent on soot surfaces.

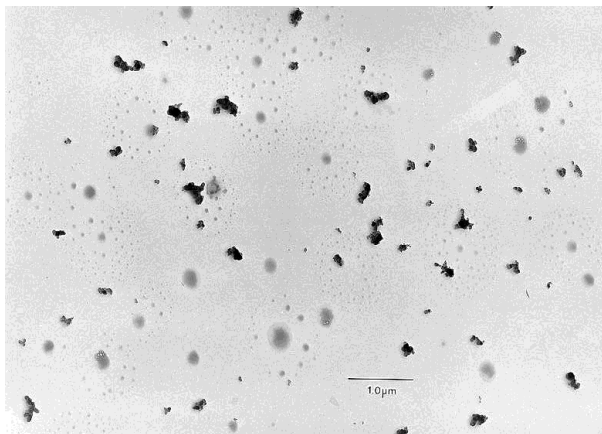


Figure 3.3: Exhaust particles in the plume of an F-16 aircraft in flight. Photomicrograph taken with a transmission electron microscope. Figure by P. Sheridan downloaded from the web site: www.cmdl.noaa.gov/aerosol/about/sheridan/particles.html.

Figure 3.3 shows an electron microscope photograph of a soot and H_2SO_4/H_2O particle mixture from in situ measurements in exhaust plumes. Soot and aqueous H_2SO_4

particles (seen as faint spherical droplets) are visible in this sample, and sulphur has been detected in/on some of the soot particles, indicative of soot and sulphur interaction in young plumes which eventually leads to an internal aerosol mixture. The degree of mixing depends on plume age and concentration of background particles, among other factors. The large sulphate droplets are background particles entrained into the plume. The photograph also reveals the irregular structure of the larger soot particles (agglomerates).

Production of soluble material by soot and SO_2 interaction is only possible by assuming perfect sticking of SO_2 molecules and rapid heterogeneous conversion to sulphate on the carbon surfaces. However, sticking probabilities of gaseous SO_2 on amorphous carbon are too small to lead to significant surface coverages and timescales in young exhaust plumes seem too short to allow heterogeneous H_2SO_4 production. However, SO_3 and H_2SO_4 molecules might easily adsorb on soot prior to volatile particle formation, and direct emissions of S(VI), as suggested by recent observations, may explain the measured soluble mass fractions on soot. Scavenging of small volatile droplets constitutes another soot activation pathway.

An impression how a soot particle coated with a small $\text{H}_2\text{SO}_4/\text{H}_2\text{O}$ droplet looks like is given by Figure 3.4. In a laboratory experiment, described in more detail by Kärcher et al. [1996], an aqueous droplet with an H_2SO_4 mass fraction of about 45% was placed onto the surface of a commercially available graphite laminate (mimicking a soot surface). The surface shown in panel a was chemically untreated, the one shown in panel b was oxidised by OH radicals such that the product of OH number density and exposure time was similar to or higher than that in aircraft plumes. While the contact angle was about 64° in the untreated sample, it decreased to 55° in the case of the OH-treated

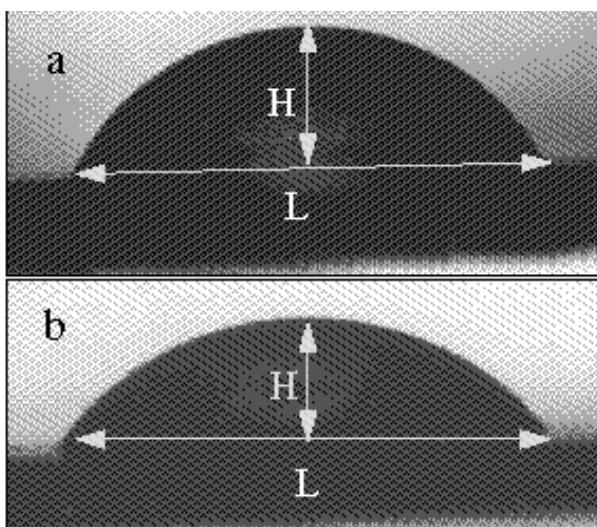


Figure 3.4: Microscope photography of a 1 mm $\text{H}_2\text{SO}_4/\text{H}_2\text{O}$ solution droplet on (a) graphite laminate and (b) graphite laminate chemically treated with OH radicals. The contact angle between the droplet and the graphite surface decreases by 10° as the surface becomes more hydrophilic due to OH radical oxidation. Figure courtesy of Uta Biermann, taken from Kärcher et al. [1996].

graphite surface. This implies that the oxidation processes lead to a more hydrophilic surface, supporting the ideas noted above.

One must bear in mind, however, that according to these results, even activated carbonaceous surfaces do not show a good compatibility with the acidic solution. As a consequence, binary heterogeneous nucleation rates are found to be several orders of

magnitudes smaller than homogeneous gas-to-particle conversion under plume conditions. Both rates become comparable only for substrates with a much higher compatibility than suggested by the described laboratory experiment.

This result is at first sight surprising because from atmospheric considerations one would expect heterogeneous nucleation to dominate homogeneous nucleation under all conceivable circumstances. However, in the young plume conditions are very extreme. The supersaturations reach much higher values than in the unperturbed atmosphere and this leads to a very small free energy of germ formation. Hence, during nucleation the system does not gain much energy even if a perfectly suitable surface is available.

Chapter 4

Conceptual Model of Contrail Formation

Because volatile particle formation and soot activation in fresh plumes was observed to depend on the fuel S content, and because contrails form on these aerosols, it was astonishing to discover that contrail formation does only weakly depend on this parameter, as presented in Figure 4.1. It is the purpose of this chapter to introduce a simple conceptual model of contrail formation that is capable of explaining the early onset of contrails and reveals the key parameters such as ice crystal sizes and optical depths that characterise young contrails. Hereafter, we apply this concept to contrails observed behind the ATTAS aircraft [Busen and Schumann, 1995].



Figure 4.1: The ATTAS contrails seen from the Falcon aircraft at ~ 100 m distance. They form within about one wingspan behind the aircraft, in this case 25–35 m behind the engines. The sulphur (S) content was 170 (5500) ppm in the left (right) engine [Schumann et al., 1996]. The right-hand contrail becomes visible slightly earlier than the left one. In a similar experiment using fuel with 2 ppm and 260 ppm S, no visible difference in the contrails was detected [Busen and Schumann, 1995].

The temporal evolution of single, spherical, small (micron-size) ice crystals that grow in an ice-supersaturated environment, such as contrails or cirrus clouds, can be obtained in analytical form by considering the H_2O mass balance and the mass growth rate of the

particles [Kärcher and Solomon, 1999]. The overall mass balance reads $IWC_{\max} = IWC_0 + m_w n_{\text{sat}} s_0$, in terms of the ice water content $IWC = \rho V$, with the ice mass density ρ and the specific ice particle volume $V = 4\pi n r^3/3$, the number density n of ice particles, the mass m_w of a water molecule, the H_2O saturation number density n_{sat} over ice, and the supersaturation $s = (n_w/n_{\text{sat}}) - 1$. The subscripts 0 and max denote initial and maximum values, respectively. From the conservation of H_2O mass, we deduce

$$s(r) = \frac{4\pi\rho n}{3m_w n_{\text{sat}}} (r_{\max}^3 - r^3), \quad (4.1)$$

and the final ice particle radius after the supersaturation relaxes to zero is given by

$$r_{\max} = \left(r_0^3 + \frac{3m_w n_{\text{sat}}}{4\pi\rho n} s_0 \right)^{1/3}. \quad (4.2)$$

The diffusional growth law for the mass per ice crystal, $m = IWC/n$, reads $dm/dt = 4\pi D r m_w n_{\text{sat}} s$, with the effective diffusion coefficient D for H_2O molecules in air taking into account the effect of gas kinetics on the molecular flux to the particles. (Ventilation corrections important for crystals much larger than those considered here, and release of latent heat, which may lead to an increase of the temperature of the particles, are not considered.) In terms of the particle radius, the growth law reads

$$\frac{dr}{dt} = \frac{m_w}{\rho} n_{\text{sat}} \frac{D(r)}{r} s(r), \quad (4.3)$$

assuming constant temperature during growth. D can be approximated by

$$D(r) = D_0 \left(1 + \frac{4D_0}{\alpha \bar{v} r} \right)^{-1}, \quad (4.4)$$

where $D_0(p, T)$ is the uncorrected diffusion coefficient, \bar{v} is the molecular thermal speed, and α is the deposition coefficient for H_2O molecules impinging on an ice surface. D_0 is connected to the molecular mean free path Λ by the gas kinetic relationship $D_0 = \bar{v}\Lambda/3$. Defining $x = r/r_{\max}$ and $\tau_g = t/t_g$, with the growth timescale t_g (as a measure of growth governed by pure gas phase diffusion) given by

$$t_g = 3/(4\pi n D_0 r_{\max}), \quad (4.5)$$

and substituting s from (4.1) and D from (4.4) in (4.3) yields

$$\tau_g(x) = \int_{x_0 \geq 0}^{x \leq 1} dx \frac{x(1 + \beta/x)}{1 - x^3}, \quad \beta = \frac{4\Lambda}{3\alpha r_{\max}}. \quad (4.6)$$

The scaled form of the integral reveals that the solutions only depend on the dimensionless parameter β and on x_0 . The integral is solved using the method of partial fractions. With the functions

$$\mathcal{I}_1(x) = \frac{1}{6} \ln \left[\frac{1+x+x^2}{(1-x)^2} \right], \quad \mathcal{I}_2(x) = \frac{1}{\sqrt{3}} \arctan \left(\frac{1+2x}{\sqrt{3}} \right), \quad (4.7)$$

the result reads

$$\tau_g(x) = (1 + \beta) [\mathcal{I}_1(x) - \mathcal{I}_1(x_0)] + (\beta - 1) [\mathcal{I}_2(x) - \mathcal{I}_2(x_0)]. \quad (4.8)$$

The result for a particular case can be obtained from this scaled solution after conversion to physical units. With Eq. 4.8 we derived a convenient expression to compute the growth history $r(t)$ of the ice crystals for a given initial radius and supersaturation.

We now return to the observations of contrail onset behind the ATTAS aircraft, as discussed by Busen and Schumann [1995]. To explain these observations we have to answer the basic question: How many ice crystals must be present initially in the plume in order to observe a visible contrail within 25 – 35 m (similar to those shown in Figure 4.1)? This may be translated into a time constraint for the solutions Eq. 4.8 from which a lower bound for n (the number of initial contrail ice particles) may be derived: the ice crystals have to grow to a visible size within 0.2 – 0.3 s, using the true airspeed 115 m s⁻¹ of the ATTAS aircraft. Next, the term “visibility” has to be quantified. The optical depth τ can be defined by

$$\tau(t) = \pi r^2(t) Q_{\text{ext}}(r) \cdot n \ell, \quad (4.9)$$

with the extinction (essentially scattering) efficiency $0 \leq Q_{\text{ext}}(r) \leq 4$, which we take from Mie-calculations for spherical ice particles with a refractive index 1.311 at a photon wavelength of 0.55 μm , and the contrail thickness ℓ . The value $\ell = 1.5$ m is a reasonable estimate for the jet diameter approximately 30 m behind the engine exit. Visible but faint cirrus clouds are characterised by $\tau_v > 0.03$, depending on wavelength, illumination conditions, viewing angle, and distance. Hence, optical depths larger than this lower limit serve as our visibility criterion.

Figure 4.2 presents the temporal evolution of the contrail’s optical depth for $r_0 = 0.02 \mu\text{m}$, $\alpha = 0.1$, and for ice particle number densities n ranging from $10^3 - 10^7 \text{ cm}^{-3}$ (solid curves) [Kärcher et al., 1996]. Other quantities such as temperature, pressure, humidity etc. have been constrained either by the observations or by fluid-dynamical calculations. The vertical dashed line indicates the time $t_v = 0.3$ s within which the contrail is first observed. For small values of n , the crystals need a relatively long time to grow to sizes large enough to impact the optical depth, the evolution

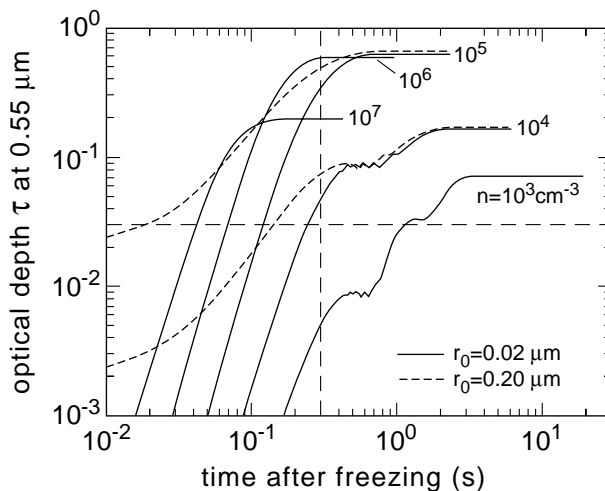


Figure 4.2: Optical depths of an aircraft contrail versus time after freezing for various ice particle number densities with initial radius 0.02 μm (solid curves) and 0.2 μm (dashed curves). For the contrail to become visible as observed, the optical depth has to pass the visibility threshold (horizontal dashed line) within 0.3 s or 35 m distance past freezing (vertical dashed line).

of which reflects the oscillating behavior of the Mie scattering function Q_{ext} with increasing r . The maximum optical depths increase with increasing values of n , although the maximum radii become smaller. This behavior is reversed for $n > 10^5 \text{ cm}^{-3}$ and $r_{\text{max}} < 0.6 \mu\text{m}$, when the particle radius becomes too small and scattering is less effective. The horizontal dashed line marks the value τ_v required for visibility. The dotted curves for $n = 10^4 \text{ cm}^{-3}$ and $n = 10^5 \text{ cm}^{-3}$ were obtained with $r_0 = 0.2 \mu\text{m}$, showing that this choice has a significant influence on the evolution of τ for times $< 0.3 \text{ s}$ after freezing. We note in passing that for r_0 significantly smaller than 20 nm , the initial growth phase would last longer because such particles would be less supersaturated. Freezing nucleation is inhibited for particles with radii smaller than $\simeq 2 - 4 \text{ nm}$.

From Figure 4.2 we conclude that around 10^4 cm^{-3} particles with sizes larger than about 20 nm must have been present initially in order to grow to a visible contrail within the time window given by the ATTAS observations. This lower bound could be somewhat relaxed (by about a factor 2) if we allow for larger particles. (When setting $\alpha = 1$ or $\alpha = 0.04$, the lower bound is shifted to 10^3 cm^{-3} or 10^5 cm^{-3} , respectively.)

Detailed numerical simulations of contrail formation and growth [Kärcher et al., 1998] support the above conclusions obtained with a rather simple phenomenological model. Especially, they show that the mean sizes of contrail ice particles increase and their number densities decrease with falling ambient temperatures and rising fuel S content. However, as observed, the contrail properties do not strongly depend on these parameters because ice formation and growth is a self-limiting process and depletion of gaseous H_2O prevents further nucleation when the concentration of ice particles exceeds the threshold of about 10^5 cm^{-3} .

The main difference between the phenomenological model discussed here and the numerical simulations is that in the former, it is assumed that the particles freeze and grow as water ice particles to their final size. In contrast, the simulations suggest that the plume aerosols first become activated into water droplets (we recall that liquid water saturation is reached or surpassed in contrails) and freeze shortly thereafter. In fact, the conjecture that the aerosol precursors first have to pass a liquid growth stage prior to freezing is in better agreement with observations [Jensen et al., 1998a].

However, the picture changes when one assumes that the aerosol precursors are perfect ice nuclei. In such a case, the liquid growth stage is not anymore required and contrails would form whenever ice saturation is reached in the plume, corresponding to the assumption made in the phenomenological model. The plume would stay longer above ice saturation, allowing more ice particles to be nucleated. Such a case could for example be realised by artificially seeding the exhaust plume with ice nuclei. Then, according to Figure 4.2. if more than about 10^8 particles per cm^{-3} froze in the exhaust plume, the contrail would actually stay invisible. This is because the mean particle size shrinks to values below about $0.06 \mu\text{m}$. At such small radii, the Mie scattering cross-section becomes very small and overcompensates the increase in particle number density. Although the contrail visibility could be dramatically reduced in this way, one risks the danger that the huge number of additional ice-forming particles efficiently trigger the formation of extended cirrus clouds after emission.

Chapter 5

Contrail Properties and Freezing Mechanisms

This chapter summarises microphysical properties of ice particles that have been obtained both from in situ measurements and from comprehensive numerical simulations. The various freezing pathways in contrails are also discussed.

According to in situ measurements using optical particle counters [Petzold et al., 1997], young contrails (plume age 5 – 20 sec) have ice particle number densities of $10^4 - 10^5 \text{ cm}^{-3}$ and mean diameters in the range 1 – 2 μm . These observations are in excellent agreement with the findings presented in the last chapter and with more detailed numerical simulations. While the optical sensors employed in the earliest contrail measurements suffered from saturation of particle counts, and could therefore not be used to measure contrails at smaller plume ages, very recent observations with

improved instruments confirm that particle numbers increase toward smaller plume ages below one second [Schröder et al., 2000a], as suggested by the models. A size distribution of such a nascent contrail measured in situ is shown in Figure 5.1.

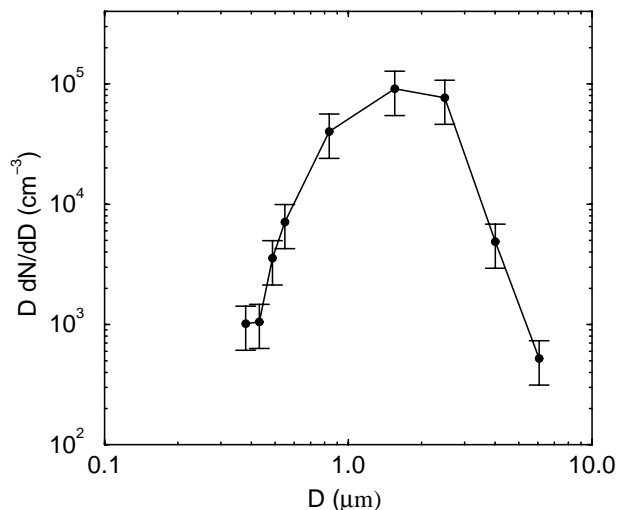


Figure 5.1: Ice particle size distribution and associated measurement uncertainties in a nascent contrail observed with an optical spectrometer in the plume of a B737 burning low sulphur fuel (2 ppm by mass). Data courtesy of Franz Schröder, adapted from Schröder et al. [2000a].

We mention two typical examples of contrail properties derived from such in situ measurements. In the case shown in Figure 5.1, the contrail was observed at a plume age of 0.4 s, about 100 m behind a B737 aircraft. The contrail contained $5 \times 10^4 \text{ cm}^{-3}$ particles with a number mean diameter of 1.5–2 μm . The surface area density was $5 \times 10^5 \mu\text{m}^2 \text{ cm}^{-3}$ and the ice water content was 170 mg m^{-3} . In another case, a contrail was observed behind the ATTAS at a flight distance of 1800 m, corresponding to a plume age of about 10 s. Number densities and mean diameters of the contrail particles measured in the dense core portion of the plume were 1500–2000 cm^{-3} and 1–1.2 μm , surface area density and ice water content were about $2000 \mu\text{m}^2 \text{ cm}^{-3}$ and 2 mg m^{-3} , respectively.

The differences between the numbers at different plume ages are mainly caused by dilution, indicating that the initial contrail growth process is finished very rapidly. (The noted ice water content may be subject to larger errors than number and surface area due to the poor counting statistics at large particle sizes). Later, the growth of ice particles may continue, but with successively slower rates and governed by the degree of supersaturation present in the ambient atmosphere, as discussed in more detail in Chapter 7.

At the plume edges, fewer but somewhat larger (factor 2) ice particles have been measured. This interesting detail underlines the fact that ice particle properties within and at the edge of young contrails systematically differ from each other. Ambient aerosols may play a role in contrail regions that nucleate at the plume edges, where the ratio of ambient to plume particles is largest and where supersaturations can remain high when ambient temperatures are sufficiently low. In fact, metal particles have been found in contrail ice crystals larger than 4–6 μm in diameter [Twohy and Gandrud, 1998], but these particles are numerically unimportant compared with other plume particles.

In principle, the observations support the model simulations that predict an increase of initial ice particle concentrations from 10^4 cm^{-3} to 10^5 cm^{-3} and a decrease of mean diameters from 2 μm to 0.6 μm when the ambient temperature is lowered by 10 K from a typical threshold formation value of 222 K [Kärcher et al., 1998]. As noted before, these numbers do not strongly depend on the fuel S content. The simulations further suggest that contrails would also form without soot and sulphur emissions by activation and freezing of background particles, which are much less abundant than aircraft-produced particles. Therefore, the resulting contrails would contain larger particles. (We recall that after all emitted water vapour has been taken up by the ice particles, their mean diameter scales in proportion to $n^{-1/3}$, because the total ice water content is invariant due to the fixed H_2O emission index.) As a consequence, there is no obvious way to avoid or suppress contrails, except by seeding the plume with additional particles (confer the last paragraph in the previous chapter).

Gierens and Schumann [1996] report a visible difference of colours of contrails with low and very high fuel S content. They explain this difference by a shift of the mean diameter of the ice particles from 1.5 μm to 0.7 μm , respectively. The simulations performed by Kärcher et al. [1998] confirm their explanation, suggesting that a combination of heterogeneous freezing of coated soot particles and additional homogeneous freezing of volatile solution droplets (in the case of very high fuel S content) is responsible for the colour change. The simulations further confirm the conjecture of Schumann et al. [1996] that an increase of the fuel S content leads to a faster growth of the liquid coatings due to enhanced uptake of H_2SO_4 prior to freezing. Enhanced H_2SO_4 masses on the soot surfaces lead to faster freezing of the liquid coatings.

Both homogeneous and heterogeneous freezing processes are possible in contrails. The most efficient freezing mode takes up the available (emitted) H_2O and prevents growth of other particle modes. Soot is expected to play an important role in the formation of contrails at and down to a few K below the threshold formation temperatures. Contrails observed under such conditions are explained to result from freezing of ice within water-activated soot particles. Volatile droplets are then prevented from freezing because the freezing of soot-containing particles is too rapid.

Fresh soot particles do not act as efficient ice deposition nuclei in the exhaust because their surfaces are not well suited to initiate the direct gas-to-solid (ice) phase transition. This follows from the absence of contrails at temperatures above the liquid water saturation threshold. Water activation of soot may result from the formation of at least a partial coating of the soot surfaces with aqueous H_2O . Prior to contrail formation, this surface coverage increases with the fuel S content and leads to a greater number of ice particles. The acid coating will persist at the soot particle surfaces. Figure 5.2 sketches the heterogeneous freezing pathway leading to contrails.

Contrails formed at threshold conditions and very low (2 ppm by mass) fuel sulphur content contain soot particles with H_2SO_4 surface coverages of only 0.02% [Kärcher, 1998b], which raises the question whether the soot activation by sulphur gases supports heterogeneous freezing in such cases. This may point towards the formation of a pure water coating (dashed arrow in Figure 5.2) that is enhanced when the fuel sulphur level is increased to average values or higher. Such a process could explain the observed insensitivity of contrail formation and visibility to changes of the fuel S content for very low sulphur levels. The formation of a (partial) liquid H_2O coating may be facilitated by both physical (adsorption due to an inverse Kelvin law effect in concave surface features) and chemical (hydrolyzable, oxygen-containing functional groups and other polar adsorption sites to which water molecules are bonded) mechanisms.

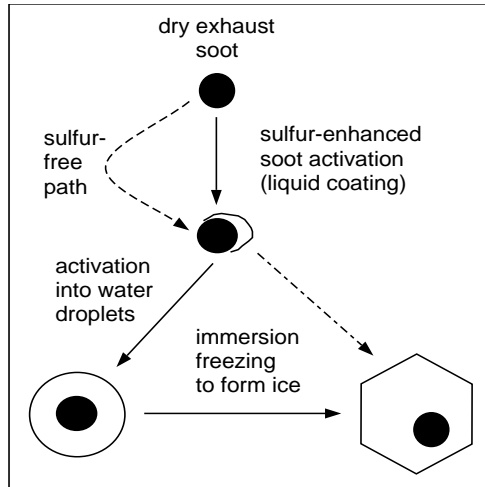


Figure 5.2: Soot-induced freezing (heterogeneous) pathway leading to contrails. Soot particles acquire a (partial) liquid $\text{H}_2\text{SO}_4/\text{H}_2\text{O}$ coating due to adsorption of oxidised sulphur gases and scavenging of volatile droplets. They also trigger freezing if the fuel S content is very low (a few ppm by mass), suggesting an additional sulphur-free heterogeneous freezing mode (dashed arrow). Few ice particles may also nucleate without water activation (dot-dashed arrow). Soot dominates ice formation at and slightly below threshold formation temperatures. Homogeneous freezing may also occur and enhance the ice mass for lower temperatures and/or higher fuel S contents (not shown). Ice crystal shapes are close to spherical in young contrails, but may vary in aging contrails as indicated by the hexagon. Soot cores may reside inside the crystals, or are attached at their surface.

The mechanism of heterogeneous ice formation via liquid coatings on soot is mainly inferred indirectly from the observations and needs experimental confirmation. Unique evidence that soot is involved in ice formation is difficult to obtain from in situ measurements, because it is difficult to distinguish whether a soot particle caused freezing or whether it was scavenged by an ice particle that formed from homogeneous freezing. The first direct evidence was found in very young contrails which evaporated quickly: part of the evaporating ice crystals released their core particles into the plume and this caused an increase in the number of soot particles counted [Schröder et al., 1998]. Due to the short time available between freezing and evaporation, the ice particles very likely formed on the soot cores, and soot scavenging by ice was inefficient.

An airborne field observation supports the notion that aircraft exhaust does not contain significant numbers of efficient ice-forming nuclei active at temperatures above 240 K [Rogers et al., 1998]. A recent laboratory investigation of ice formation by black carbon particles shows that coated soot exhibits a high barrier to freezing also below 230 K, but triggers the phase transition more efficiently than volatile sulphate solutions at sufficiently low temperatures [DeMott et al., 1999]. Chemically untreated soot particles showed a poor activity as deposition ice nuclei, pointing to the existence of a sulphur-free freezing path as indicated by the dot-dashed arrow in Figure 5.2. Particles with an approximate monolayer coverage by H_2SO_4 nucleated ice at humidities consistent with homogeneous freezing of the $\text{H}_2\text{SO}_4/\text{H}_2\text{O}$ layer. Particles with thicker coatings froze as solution droplets somewhat more readily than homogeneous freezing would predict: the heterogeneous freezing thresholds in this case dropped from values near water saturation (relative humidity over ice of about 160 %) at temperatures above 223 K to values 76-82 % relative humidity with respect to water (corresponding to about 130 % over ice) at 213 K.

Of course, as in previous laboratory studies, the implications for the role of soot in forming contrails or cirrus clouds depend on how representative the described nucleating behaviours of the employed carbonaceous particles are of jet exhaust soot. Nevertheless, the freezing scenario suggested by these data is strikingly similar to the proposed theoretical scenario depicted in Figure 5.2.

The fraction of frozen volatile $\text{H}_2\text{SO}_4/\text{H}_2\text{O}$ droplets depends on the droplet composition (affecting homogeneous freezing rate), the evolution of H_2O supersaturation, and the possible competition with heterogeneous freezing processes involving soot. Near the threshold conditions, model results suggest that the volatile aerosol fraction does not become large enough to freeze [Kärcher et al., 1995; 1998], and heterogeneous freezing of activated soot particles initiates contrail formation. We explain this now in more detail.

The homogeneous freezing rate J of the volatile $\text{H}_2\text{SO}_4/\text{H}_2\text{O}$ droplets is an extremely sensitive function of the H_2SO_4 mass fraction W and the temperature T . Figure 5.3 presents the temperature-composition diagram for this binary system under plume conditions. These are chosen such that water saturation is approached but not reached (the peak plume relative humidity is 95 %, the ambient temperature of 224 K stays slightly below the threshold formation temperature at an ambient pressure of 240 hPa and humidity of 63 %). The thin solid curves are the melting point curves for ice and several hydrates of H_2SO_4 . The W - T -histories of droplets in the plume with radii 0.4, 1, 4, and ≥ 100 nm are shown as thick solid curves and the right ordinate marks the corresponding plume age.

The freshly nucleated droplets have H_2SO_4 mass fractions ranging from 0.7–0.8, depending on the germ radius. Figure 5.3 clearly reveals that, because of the Kelvin effect¹, larger droplets condense and dilute markedly faster than smaller ones. For the total simulation time of 10^3 s, the small droplets with $r < 2$ nm stay highly acidic and end up as supercooled liquid with mass fractions $W > 0.4$ after experiencing a growth and shrink cycle. In contrast, the droplets with $r \geq 4$ nm enter the freezing region. However, only the droplets with radii $r \geq 100$ nm experience homogeneous freezing rates $J = 10^{15} \text{ cm}^{-3} \text{ s}^{-1}$ (per unit droplet volume per second), leading to reasonably short freezing timescales $t_{\text{frz}} = 3/(4\pi r^3 J) \leq 0.25$ s. For $n(r \geq 40 \text{ nm})$, it follows $t_{\text{frz}} \leq 40$ s. However, we note that the number densities of droplets with radii $r \geq 40$ nm and $r \geq 100$ nm remain insignificant during the total simulation time (not shown here).

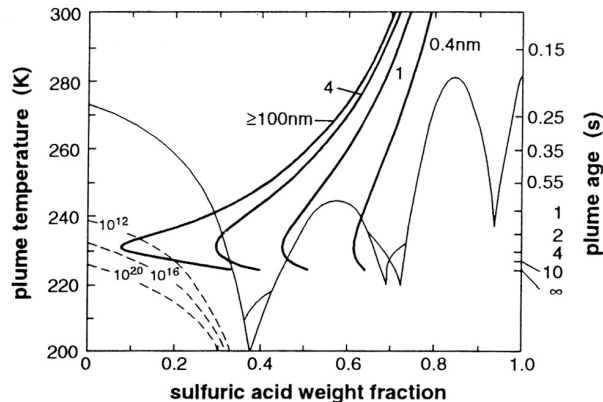


Figure 5.3: H_2SO_4 mass fractions of solution droplets with different radii (thick solid curves) as they evolve with temperature (left axis) and corresponding plume age (right axis). The dashed contour curves below the ice-liquid coexistence curve mark homogeneous freezing rates per unit droplet volume per second ($\text{cm}^{-3} \text{ s}^{-1}$). The thin solid curves represent the melting point curves for ice and several H_2SO_4 hydrates. Only larger droplets enter the freezing region.

The above discussion underscores that homogeneous freezing of volatile $\text{H}_2\text{SO}_4/\text{H}_2\text{O}$ droplets is not likely to account for sufficient ice particle production under condition close to the formation threshold temperature. This picture does not change when uncertainties in the homogeneous binary nucleation and plume mixing rates are considered, and hold even for a very high fuel S content of 3 g S/kg fuel [Kärcher et al., 1995], and when the effects of chemi-ions is taken into account [Kärcher et al., 1998]. The model predicts contrail formation by this mechanism only if the plume becomes water supersaturated, in which case homogeneous freezing competes with soot-induced freezing processes and also ambient particles may contribute to ice crystal nucleation.

In the temperature regime well below the formation threshold, $\text{H}_2\text{SO}_4/\text{H}_2\text{O}$ droplets larger than the threshold activation size (radii $> 2 - 5$ nm) can be activated into water droplets in the contrail. The threshold activation size and, hence, freezing probability, depends on the maximum supercooling reached in the expanding plume. Decreasing ambient temperature and increasing ambient humidity both lower the threshold size and increase the homogeneous freezing rates. In this regard, volatile particles from the ion mode are more easily activated than those from the neutral mode, and, hence, play an important role in contrail formation [Yu and Turco, 1998].

¹The vapour pressure of gases over particles increases with decreasing particle size (Kelvin effect). This implies that larger supersaturations are required for molecules in smaller particles to maintain equilibrium with the gas phase. Further, the solubilities of gases in liquid phase droplets become reduced with decreasing size, because the solubilities depend on the vapour pressures.

Chapter 6

Processing of Aerosols in Contrails

The evolution of volatile particles in young plumes differs strongly in contrails from conditions in dry plumes. As explained in the previous chapter, part of the volatile particles grow by water uptake and may then freeze. The ice particles grow in surface area due to deposition of H_2O and efficiently scavenge part of the volatile and soot particles during their lifetime, even in short-lived contrails. As a consequence, contrails contain fewer of the small particles than dry plumes [Anderson et al., 1998; Schröder et al., 1998]. After evaporation of the ice crystals, the residual soot and sulphate cores are returned to the atmosphere.

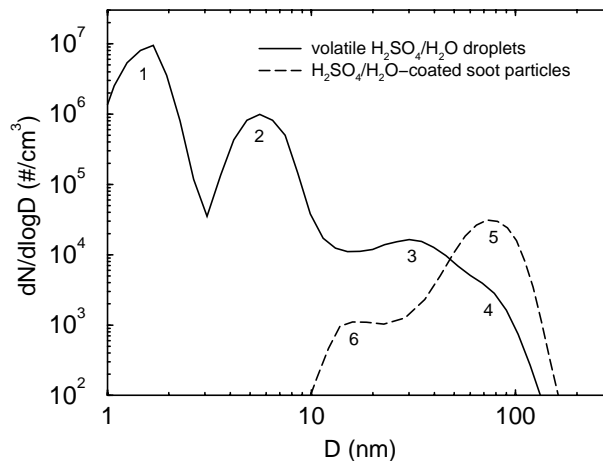


Figure 6.1: Simulated size distributions of acid (solid curve) and mixed soot/sulphate particles (dashed curve) in an evaporating short-lived contrail in a high sulphur plume at about 20 s plume age. Numbers denote distinct modes in the particle spectra, caused by coagulation processes between these particles and the contrail ice crystals. Data courtesy of Fangqun Yu, adapted from Yu and Turco [1998].

Particle processing in (short-lived) contrails likely leads to a modified aerosol size spectrum and probably composition [Yu and Turco, 1998], similar to the effect cloud processing is known to have on aerosol properties. Figure 6.1 depicts particle spectra in an evaporating contrail from a simulation model. Both acid and coated soot particle size distributions exhibit distinct modes. Mode 1 and mode 2 represent the neutral and

ion mode, respectively, after processing occurred at a plume age of 20 s. (We recall that the unperturbed modes are depicted in Figure 3.2 at a plume age of 1 s.) Mode 3 at a diameter of ~ 30 nm is an activation mode resulting from water uptake by the largest of the ion mode aerosols; these aerosols did not freeze. Mode 4 at 80 nm is an accumulation-type mode that was processed through the ice crystals, that is, these particles went through a freezing-evaporation cycle. The soot modes 5 and 6 are created analogous to modes 4 and 3, respectively.

As conjectured by DeMott et al. [1999] on the basis of laboratory freezing experiments, the residual particles from evaporating contrails might be more efficient ice nuclei for cirrus formation than fresh, more hydrophobic soot. But even without formation of contrails, aircraft soot and sulphate particles enhance the atmospheric aerosol in terms of number and surface area densities [Kärcher and Meilinger, 1998; Yu and Turco, 1999; Anderson et al., 1999]. If only a small fraction of the abundant volatile particles were to grow to sizes sufficient to act as cloud condensation or ice nuclei, or the coated soot particles are more efficient freezing nuclei than the background particles, they could have important climatic implications.

However, to track the evolution of aircraft particulates in the aging plume over the timescale of days is a difficult problem, depending on the availability of atmospheric SO_2 and particles, among other details. It is noteworthy that, according to detailed microphysical simulations for relatively clean upper tropospheric conditions, reductions in the fuel S content may not efficiently reduce the number of climatically significant particles injected into by aircraft [Yu and Turco, 1999]. Unfortunately, the importance of such perturbations cannot be quantified at this time, mainly due to the lack of atmospheric measurements.

Chapter 7

Impact of Aircraft Particulates on Cirrus

Soot particles originating from aircraft exhaust may act as freezing agents and form cirrus clouds under atmospheric conditions where otherwise no cloud would form. Such a perturbation could lead to an expansion of cirrus cover, changes of microphysical and optical properties of clouds, and the associated radiative forcing [Jensen and Toon, 1997]. In situ measurements of upper tropospheric cirrus clouds in regions with dense air traffic have clearly shown an enhancement of the ratio between ice crystal and aerosol number densities in regions of cirrus where the crystals contain relatively high amounts of absorbing material, presumably aircraft-derived soot [Ström and Ohlsson, 1998]. Specifically, for the same number of aerosol particles, perturbed clouds contained 1.6 to 2.8 times more ice crystals than unperturbed clouds. This result suggests that the enhanced crystal concentrations are linked to aircraft soot emissions. The detailed mechanism causing this enhancement cannot be inferred from the observations.

For aircraft to alter cirrus properties, exhaust soot particles would need to be more efficient ice nuclei than the background particles existing within the same air mass. If the predominant atmospheric particles that freeze to form ice are composed of liquid $\text{H}_2\text{SO}_4/\text{H}_2\text{O}$, aircraft soot particles could exert an impact on cloud formation at low temperatures ($< 220 \text{ K}$) if they exhibit the same freezing properties as the carbon surfaces investigated in the laboratory [see DeMott et al., 1999 and recall the discussion in Chapter 6], because sulphate particles require a relatively high supersaturation before freezing occurs [Koop et al., 1999]. If the predominant atmospheric particles that freeze are good freezing nuclei, then soot from aircraft will have a small, if any, impact on cirrus. The number of such heterogeneous freezing nuclei that are active at warm ($> 230 \text{ K}$) temperatures is not always small in the upper troposphere, as demonstrated by DeMott et al. [1998]. The magnitude and importance of such potential modifications is currently not well understood.

Cirrus clouds may also be modified by enhanced sulphate aerosols, but only larger particles ($> 50 - 100 \text{ nm}$) are efficient. Such large particles may originate from ambient particles enlarged by growth from H_2SO_4 (via aircraft-emitted or ambient SO_2) or by processing of liquid aerosols in short-lived contrails (for example as shown in Figure 6.1). It is well-known from model studies that large sulphate particles, such

as those produced within the Mount Pinatubo volcanic cloud, could lead to a significant increase in number of ice crystals, optical depth, and radiative forcing of cirrus. Such modifications would predominantly occur in cold cirrus (<220 K), weakly forced by slow updrafts, and would require a large increase in the number of large sulphate particles.

Observations from space [Minnis et al., 1998] and in situ measurements [Schröder et al., 2000b] clearly show that persistent contrails may develop into cirrus clouds, thereby approaching size distributions as typically observed in young cirrus on timescales of up to a few hours. The contrails with the longest lifetimes and the largest horizontal coverage have the greatest potential for affecting regional or global climate.

Contrail persistence is primarily linked to synoptic conditions that support vertical motions of air, such as frontal zones connected with the warm sector of lows, jet streams that carry moist air across stable highs, and flows induced by mountain waves. These conditions may ensure that the relative humidity exceeds ice saturation, promoting depositional growth of the contrail crystals. Contrail ice crystals evaporate quickly when the ambient air is subsaturated with respect to ice, unless the particles are coated with certain substances such as HNO_3 [Diehl and Mitra, 1998]. Contrail spreading may be induced by vertical wind shear, especially in contrails with a large vertical extent caused by updrafts driven by radiative heating.

In Figure 7.1 we show a representative selection of observed particle concentrations illustrating the transition of contrails into cirrus clouds [Schröder et al., 2000b]. The contrails were sampled in the upper troposphere over Germany at altitudes between 9.5 and 11.5 km. Shown are a fresh contrail (labelled AT), an evaporating short-lived contrail (A), few minutes old, persistent contrails (A1, A2), one older than 15 minutes (O) and one older than 30 minutes (U). For comparison, soot emissions (taken in an exhaust plume where no contrail formed) and a young cirrus cloud mode are also shown with labels S and Cf, respectively.

Contrails with progressively increasing age (from AT to U) exhibit a continuous decrease of ice crystal concentrations from $> 2000 \text{ cm}^{-3}$ to about 10 cm^{-3} caused by plume dispersion. At the same time, their mean diameters increase from initially $1 \mu\text{m}$ to about $8 \mu\text{m}$, within the timescale of about 30 minutes to 1 hour, close to the typi-

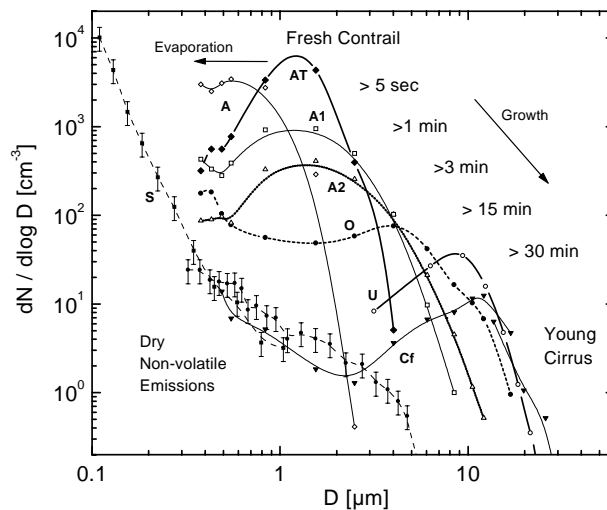


Figure 7.1: Representative selection of observed size-resolved particle concentrations illustrating the transition of contrails into young upper tropospheric cirrus clouds. S: exhaust soot spectrum in a plume without contrail. A: Evaporating, short-lived contrail. Cf: Young cirrus cloud. Others: Persistent contrails at different plume ages. Figure taken from Schröder et al. [2000a].

cal size of crystals in young cirrus. The variability of observed spectra is high in the near-field. The variability is smaller at later stages, mainly controlled by ambient temperature and humidity. Observations and model estimates suggest that contrail growth is only weakly affected by preexisting cirrus on these timescales.

The growth of the ice crystals in the persistent contrails was such that the measured surface area densities of the clouds stayed approximately constant, implying that the reduction of the crystal number due to dilution effects were compensated by condensational growth of the ice crystals. Considering the observed variability in observations together with experimental uncertainties, the data suggest a range of $3500 \mu\text{m}^2 \text{cm}^{-3} \pm 40\%$ as a characteristic value for the persistent contrails on timescales of a few minutes up to an hour. Since the Mie scattering coefficient (calculated for a wavelength of $0.5 \mu\text{m}$) is only weakly varying for particles larger than a few micrometers, this implies that the optical extinction of persistent contrails is comparable to that of young cirrus (mean diameter $\sim 10 \mu\text{m}$), variable within a factor of three.

However, optical depths and radiative forcing may differ by larger factors due to different geometrical properties. Because the variability of environmental conditions and contrail ages were limited for the suite of contrails observed by Schröder et al. [2000b], contrails may evolve differently in a warmer or colder environment or over longer timescales. In situ observational evidence is poor for such cases [e.g., Heymsfield et al., 1998; Jensen et al., 1998b]. For example, the contrail described by Heymsfield et al. [1998] contained very few (< 0.1 crystals per litre) ice crystals with sizes up to $300 - 500 \mu\text{m}$ at its periphery (resembling ambient developed cirrus in this respect), in addition to the many small particles present within the contrail core. The measurements suggest that a small fraction of core particles became mixed into the supersaturated contrail edges and grew, and eventually formed precipitation streamers (virga). Jensen et al. [1998b] theoretically discussed a contrail observed at 212 K which had a complex microphysical structure. Other aspects about contrail-cirrus have been reviewed by Schumann [2000b].

While size distributions of contrail ice crystals have been measured in some detail, optical measurements of shapes and light scattering properties of the ice crystals in cirrus and contrails are likewise difficult to study with in situ observations and hardly available [e.g., Lawson et al., 1998; Gayet et al., 1998; Liou et al., 1998]. Given the wide range of environmental conditions under which persistent contrails may develop, and which have not yet been fully explored by observations, it is difficult to assess to which extent contrails and natural cirrus clouds differ from each other in terms of radiative properties. A detailed comparison is further rendered difficult because cirrus are usually highly structured, especially clouds at midlatitudes and freezing occurs sporadic and localized.

Numerical simulations of cloud formation and development can yield further information. We now review examples of numerical simulations of persistent contrails using two-dimensional cloud-resolving models. Gierens and Jensen [1998] have performed simulations of the transition of a contrail into a young cirrus cloud using measured profiles of wind and temperature in an environment slightly above ice saturation. Figure 7.2 depicts the transformation at contrail ages of 6 s, 150 s, and 30 min. Shown are contour lines of ice water content in units of mg ice per m^3 of air versus altitude (vertical axis) and horizontal extent (horizontal axis), both in metres. We remark that while the first plate (6 s) shows the two contrails as they evolve from the wing-tip vortices, the second plate (150 s) depicts water ice originating from the secondary wake. The

secondary contrail cloud forms due to upward-moving air detrained from the vortices; the vortices rapidly sink and become adiabatically compressed and heated, leading to the disappearance of the primary contrail structure. This effect has been observed by lidar measurements [Sussmann and Gierens, 1998] and appears preferentially behind heavy airliners with four engines.

The figure shows that the contrail spreads in both directions while the ice particles grow by taking up ambient water vapour. Growth in the vertical direction, even up to 400 m into a dry layer above the flight level, is strong in the first stage of contrail evolution, driven mainly by the prescribed temperature profile. After 15 min, the contrail disperses horizontally, reaching a width of 2 km at the end of the simulation. The evolution of the simulated crystal size distributions at the positions of maximum ice water content (not shown) reveals a striking similarity with those shown in Figure 7.1, achieving mean sizes of the order 10–20 μm . This increases confidence in such types of simulations.

However, some contrail ice crystals can reach much larger sizes, as noted above. Simulations of a contrail spreading and growing in a sheared environment have been presented by Jensen et al. [1998c]. In simulations with large relative humidities over ice (above 125%) – such as those frequently observed in the upper troposphere – crystals with lengths exceeding 100 μm are generated by depositional growth, in accordance with observations. These large crystals fall rapidly, and significant horizontal spreading occurs primarily as a result of crystal precipitation in conjunction with vertical wind shear. Strong radiative heating (up to 10 K per day) in the contrail region enhances vertical mixing.

These simulations highlight the need for further systematic model studies of persistent contrails. For example, ice crystal properties, contrail spatial structure and radiative heating, and generation of precipitation depend strongly on contrail and surface temperatures, ambient humidities, wind shear, the presence of clouds below the contrail, among other factors. The dependencies and the sensitivities associated with each of these parameters have not been studied in detail.

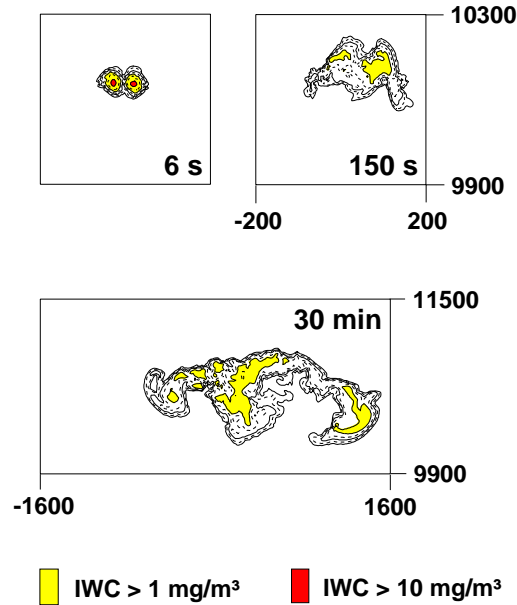


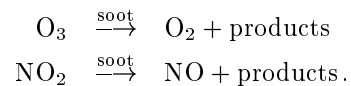
Figure 7.2: Transformation of a contrail into a cirrus cloud. Two-dimensional large-eddy simulation using observed wind and temperature profiles, assuming moderate ice supersaturations. Vertical axis: altitude (in m), horizontal axis: contrail width (in m), contour lines: ice water content (in mg/m^3). Figure courtesy of Klaus Gierens, adapted from Gierens and Jensen [1998].

Chapter 8

Impact of Aircraft Particulates on Chemistry

The three particle types present in aircraft plumes and contrails, soot particles, volatile droplets, and ice crystals, may exert different impacts on heterogeneous chemistry. We briefly describe the present state of knowledge.

Concerning aircraft soot, the following two redox reactions have been discussed in the literature:

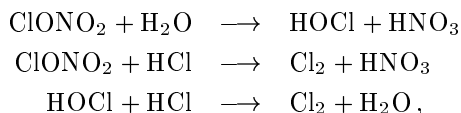


The first reaction directly destroys ozone, while the second reaction affects ozone indirectly, via the gas phase reaction of NO with O₃. Gao et al. [1998] have investigated the efficiency of these reactions that could affect atmospheric ozone using measurements of ozone in an aged aircraft plume. At a cruise altitude of 100 hPa, no significant ozone loss has been measured at plume ages up to 1 hour, as a comparison revealed between measured concentrations of O₃ and N₂O and respective concentrations derived from the well-established O₃-N₂O correlation in the lower stratosphere. An upper bound for the product of specific soot surface area density and the efficiency of the heterogeneous reactions could be derived, showing that both reactions are unimportant under upper tropospheric/lower stratospheric conditions.

These findings are in good agreement with a recent laboratory study investigating the direct reaction of ozone with soot aerosol [Kamm et al., 1999]. These investigators could show that ozone losses on soot aerosol are essentially limited to one surface layer equivalent, since a potential contribution of catalytic ozone destruction processes on the soot surfaces becomes negligible at low temperatures. However, because the mass concentration of ozone at cruise altitudes is several orders of magnitudes higher than that of soot aerosol, only a catalytic loss cycle could substantially reduce the ozone concentrations.

Next, we discuss the effects of the new volatile aerosols from aircraft on heterogeneous chemistry. Global chemical models predict significant ozone reduction in the lower stratosphere caused by the liquid particles produced in the near-field plumes of

supersonic aircraft as part of a proposed fleet operating in 2015 or later [Weissenstein et al., 1998]. In this context, the heterogeneous chlorine activation reactions



are discussed, where the reaction of ClONO_2 with HCl is of dominating influence.

Recent numerical simulations have demonstrated that on a regional scale, such as the flight corridor over the North Atlantic, liquid sulphate aerosols from aircraft (either subsonic or supersonic) cannot be expected to exert a significant impact on ozone [Meilinger et al., 2000]. Because of the Kelvin effect (see footnote in Chapter 5), the small new particles are more acidic than background particles due to a reduced solubility of H_2O , HNO_3 , and HCl under the same atmospheric conditions. This reduces their chemical reactivity, because the reaction probabilities for chlorine activation are extremely sensitive functions of the H_2O and HCl content in the sulphate droplets. In addition, at progressively decreasing temperatures, where the reactivity increases dramatically, the new particles become more rapidly scavenged by the swelling aerosol perturbation by aircraft.

In the first global studies devoted to the chemical effects of new sulphate aerosols caused by aircraft emissions, it was simply assumed that the heterogeneous chemical effect of these particles scales in proportion to the enhancement of the background aerosol surface area A , an assumption Meilinger et al. [2000] have shown not to hold. Their proposed effects limiting the chemistry on aviation-produced aerosols have not yet been considered in global chemical models. Because of the strong suppression of ozone destruction on the aircraft aerosol mode on regional scales, we expect reduced simulated ozone losses due the operation of supersonic aircraft in the global lower stratosphere.

However, even though the effect of sulphate particles from aircraft on ozone is rather small, heterogeneous chemistry might be affected by aircraft emissions. Aviation-produced H_2O and NO_x emissions could increase the threshold temperature for substantial chlorine activation on background aerosol (most relevant for supersonic aircraft in the lower stratosphere). Particles from aircraft cause persistent contrails and perhaps additional cirrus cloud formation (relevant in the upper troposphere and the tropopause region).

The above chlorine activation reactions can also take place efficiently on the surfaces of ice crystals in contrails and cirrus clouds [Borrmann et al., 1996]. While simple estimates suggest that chlorine activation may occur in contrails [Kärcher, 1997], detailed investigations with a comprehensive chemical code coupled to a microphysical model for contrail formation and evolution are still to be performed. The frequent presence of ice particle layers in the lower stratosphere has been reported by Lelieveld et al. [1999] during an airborne field mission. Currently, little is known about aerosol and cirrus properties in the tropopause region that would allow to reliably assess this issue [Kärcher and Solomon, 1999].

Chapter 9

Uncertainties, Impacts, and Future Research

We give brief answers to the key questions posed in the introduction, summarising several important conclusions of this work, discuss atmospheric impacts and uncertainties and finally propose in which directions future research should be concentrated to resolve the open issues.

How do contrails form from aerosols present in aircraft exhaust plumes ?

Young contrails consist of water ice particles that nucleate primarily on exhaust soot and volatile aerosol particles, owing to heterogeneous and homogeneous freezing processes. Contrails would also form without aircraft soot and sulphate emissions by activation and freezing of background particles.

There are no basic uncertainties related to this issue. The high number of ice particles observed in contrails necessitates that particles emitted by the engines or produced in the plume trigger contrail formation. Contrail formation in the absence of aircraft particulates is of course hypothetical and the answer relies on simulation results. However, there is no doubt that contrails would still form, albeit with different properties. The future research priority in this area should be low. If future fleets use liquid hydrogen instead of kerosene, more research is needed to investigate the contrail properties.

How accurately can we predict contrail formation ?

The thermodynamic criterion that allows to predict contrails as a function of a few atmospheric and engine-related parameters is well established and verified by in situ observations. This approach does not require physical details of contrail formation to be known.

A sufficiently large number of observations and measurements have been made to safely answer this question. Once a few atmospheric and engine-related parameters (ambient pressure, temperature, humidity; water vapour emission index, specific combustion heat of the jet fuel, engine thrust, fuel flow rate, flight velocity) are known, the appearance of contrails in the atmosphere can accurately be predicted. Of course, these parameters must be known with sufficient accuracy, which may be a problem in the case of atmospheric relative humidity. No future research is required.

What are the uncertainties in mechanisms for contrail formation ?

Uncertainties in freezing mechanisms leading to ice particles in contrails are mainly related to the poorly characterized ice-forming properties of soot particulates, and, to a lesser extent, to volatile particles produced in the plume or entrained from the ambient air.

Except near threshold formation conditions, calculated contrail properties are not sensitive to uncertainties in freezing nucleation rates because of the high supersaturations reached in the plume (which are typically above water saturation). Slight variations in ice particle number and size noted in field observations can be explained by variations in fuel sulphur contents and environmental conditions. However, the classical heterogeneous nucleation rates for coated soot particles used in some models may not represent the actual microphysical process. In the context of contrail formation, the research priority should be low.

How could changes in engine emissions affect contrail formation ?

Increasing the bypass ratio of jet engines increases their propulsive efficiency which in turn lowers the threshold temperatures for contrail formation. The use of liquid hydrogen instead of kerosene would substantially lower the formation threshold temperatures. Contrail formation cannot be avoided or suppressed, except perhaps by massively seeding the exhaust with efficient ice-forming nuclei.

Contrails forming on background aerosol particles without aircraft soot and sulphur emissions likely contain fewer, but larger ice crystals. It is conceivable that the microphysical variability of contrails forming exclusively on ambient particles is higher, because of the variability of number and freezing properties of particles in the air at cruise altitudes. However, as in the case of seeded contrails, the detailed properties of such contrails are essentially unknown. Future research would be necessary if future engines were to be fueled by liquid hydrogen.

Accurate predictions of the atmospheric impact of contrails depends on how we can reliably predict regions in the atmosphere prone to contrail formation, among other factors. Increasing the threshold temperatures increases the altitude range within which contrails form. More ice clouds appearing in the lowermost stratosphere may cause chemical perturbations affecting ozone. Lower flight levels increase fuel consumption and CO₂ and NO_x emissions. Even without changes in engine emissions, future research should concentrate on improving the predictive capability of large-scale models in terms of a better representation of the location of the tropopause, water vapour and temperature fields¹, cirrus clouds, and chemistry in the tropopause region (high research priority).

Seeding could perhaps serve as a means to minimize the radiative impact of contrails. However, the resulting enhanced particle concentrations in the atmosphere would almost certainly increase cloudiness indirectly. No future research should be devoted to this issue.

¹Note that already observed changes of water vapour mixing ratios and temperatures in the lower stratosphere caused by the greenhouse effect is a climate change issue. In the period 1980–1996, ozone declined with a trend of about $7.5 \pm 5\%$ per decade at an altitude of 15 km at northern midlatitudes [SPARC, 1998].

How much is known about persistent contrails and cirrus resulting from aircraft particulates ?

Over the timescale of one hour, persistent contrails approach particle size distributions that resemble those of young, upper tropospheric cirrus clouds at midlatitudes. It is difficult to assess to which extent contrails and natural cirrus clouds differ from each other in terms of radiative properties.

While it has been demonstrated by satellite and in situ observations that linear contrails can transform into extended cirrus cloud decks, the abundance and possible range of microphysical and radiative properties of contrail cirrus has not yet been explored. This renders reliable estimates of the associated radiative forcings and efforts to develop parameterisation schemes for use in global models difficult. To resolve this issue, future research in this field should receive high priority.

The evolution of cirrus clouds can potentially be modified by aircraft exhaust. For aircraft to alter cirrus properties, exhaust soot particles would need to be more efficient ice nuclei than the background particles existing within the same air mass. The residual particles from short-lived contrails might be more efficient ice-forming agents than fresh soot. However, the freezing behaviour of mixtures of soot and sulphate aerosols in aging plumes or processed by contrails has not yet been studied systematically. Further, sulphate aerosol enhanced or modified by aircraft emissions may also alter cirrus properties. Such modifications would predominantly occur under cold conditions and with weak dynamical forcings, and would require a large increase in the number of large sulphate particles. Because it is unlikely that aircraft sulphur emissions will cause large increases of the large background particle fraction, soot particles coated with sulphate or entrained into sulphate droplets will likely be more important in forming new or modifying existing cirrus. The research priority should be high.

What are the potential chemical effects of aviation-produced aerosols and clouds in the atmosphere ?

Chemical effects of soot and sulphate particles from aircraft at cruise seem to be insignificant, while increases in lower stratospheric water vapour due to aircraft operations may cause faster heterogeneous chemistry on background aerosol particles. Chlorine activation reactions may occur on the surfaces of ice crystals in cirrus clouds and contrails above the tropopause.

Previous models investigating potential chemical effects of supersonic aircraft in the stratosphere show a large sensitivity of computed ozone depletion to assumed properties of sulphate particles produced at emission. In the light of new results about limitations of heterogeneous chemistry on aviation-produced aerosols, these simulations should be revised. In the context of aviation, soot-related chemistry may not require further research in the near future. In contrast, heterogeneous chemistry on ice surfaces should receive high research priority, because significant potential impacts of clouds on chemical balance have been identified. In this regard, a better understanding of the role of natural cirrus in the chemistry of the upper troposphere and lowermost stratosphere is required before the chemical impact of contrails can be fully addressed.

Chapter 10

References

- Anderson, B.E., W.R. Cofer, J.W. Barrick, D.R. Bagell, and C.H. Hudgins
Airborne observations of aircraft aerosol emissions. II: Factors controlling volatile particle production
Geophys. Res. Lett., 25, 1693–1696, 1998.
- Anderson, B.E. W.R. Cofer, G.L. Gregory, S. Vay, K.E. Brunke, Y. Kondo, M. Koike, H. Schlager, S. Baughcum, and E.J. Jensen
An assessment of aircraft as a source of particles to the upper troposphere
Geophys. Res. Lett., 26, 3069–3072, 1999.
- Appleman, H.
The formation of exhaust contrails by jet aircraft
Bull. Amer. Meteor. Soc., 34, 14–20, 1953.
- Borrmann, S., S. Solomon, J.E. Dye, and B. Luo
The potential of cirrus clouds for heterogeneous chlorine activation
Geophys. Res. Lett., 23, 2133–2136, 1996.
- Busen, R. and U. Schumann
Visible contrail formation from fuels with different sulfur contents
Geophys. Res. Lett., 22, 1357–1360, 1995.
- DeMott, P.J., D.C. Rogers, S.M. Kreidenweis, Y. Chen, C.H. Twohy, D. Baumgardner, A.J. Heymsfield, and K.R. Chan
The role of heterogeneous freezing nucleation in upper tropospheric clouds: Inferences from SUCCESS
Geophys. Res. Lett., 25, 1387–1390, 1998.
- DeMott, P.J., Y. Chen, S.M. Kreidenweis, D.C. Rogers, and D.E. Sherman
Ice formation by black carbon particles
Geophys. Res. Lett., 26, 2429–2432, 1999.
- Diehl, J. and S.K. Mitra
A laboratory study of the effects of a kerosene burner exhaust on ice nucleation and the evaporation rate of ice crystals
Atmos. Environ, 32, 3145–3151, 1998.

- Gao, R.S., B. Kärcher, E.R. Keim, and D.W. Fahey
Constraining the heterogeneous loss of O₃ on soot particles with observations in jet engine exhaust plumes
Geophys. Res. Lett., 25, 3323–3326, 1998.
- Gayet, J.-F., F. Auriol, S. Oschchepkov, F. Schröder, C. Duroure, G. Febvre, J.-F. Fournol, O. Crépel, P. Personne, and D. Daugeron
In situ measurements of the scattering phase function of stratocumulus, contrails, and cirrus
Geophys. Res. Lett., 25, 971–974, 1998.
- Gierens, K. and U. Schumann
Colors of contrails from fuels with different sulfur contents
J. Geophys. Res., 101, 16731–16736, 1996.
- Gierens, K. and E. Jensen
A numerical study of the contrail-to-cirrus transition
Geophys. Res. Lett., 25, 4341–4344, 1998.
- Hagen, D.E., M.B. Trueblood, and P.D. Whitefield
A field sampling of jet exhaust aerosols
Particulate Sci. Technol., 10, 53–63, 1992.
- Heymsfield, A.J., R.P. Lawson, and G. Sachse
Development of ice particles precipitating from a contrail during SUCCESS
Geophys. Res. Lett., 25, 1335–1338, 1998.
- IPCC (Intergovernmental Panel on Climate Change) – Aviation and the Global Atmosphere. Eds.: J.E. Penner, D.H. Lister, D.J. Griggs, D.J. Dokken, M. McFarland
Cambridge Univ. Press, 373 pp., 1999.
- Jensen, E.J. and O.B. Toon
The potential impact of soot particles from aircraft exhaust on cirrus clouds
Geophys. Res. Lett., 24, 249–252, 1997.
- Jensen, E.J., O.B. Toon, S. Kinne, G.W. Sachse, B.E. Anderson, K.R. Chan, C. Twohy, B. Gandrud, A. Heymsfield, and R.C. Miake-Lye
Environmental conditions required for contrail formation and persistence
J. Geophys. Res., 103, 3929–3936, 1998a.
- Jensen, E.J., O.B. Toon, R.F. Pueschel, J. Goodman, G.W. Sachse, B.E. Anderson, K.R. Chan, D. Baumgardner, and R.C. Miake-Lye
Ice crystal nucleation and growth in contrails forming at low ambient temperatures
Geophys. Res. Lett., 25, 1371–1374, 1998b.
- Jensen, E.J., A.S. Ackerman, D.E. Stevens, O.B. Toon, and P. Minnis
Spreading and growth of contrails in a sheared environment
J. Geophys. Res., 103, 31557–31567, 1998c.
- Kärcher, B., Th. Peter, and R. Ottmann
Contrail formation: Homogeneous nucleation of H₂SO₄/H₂O droplets
Geophys. Res. Lett., 22, 1501–1504, 1995.
- Kärcher, B., Th. Peter, U.M. Biermann, and U. Schumann
The initial composition of jet condensation trails
J. Atmos. Sci., 53, 3066–3083, 1996.

- Kärcher, B.
Heterogeneous chemistry in aircraft wakes: Constraints for uptake coefficients
J. Geophys. Res., *102*, 19119–19135, 1997.
- Kärcher, B.
Physicochemistry of aircraft-generated liquid aerosols, soot, and ice particles, 1,
Model description
J. Geophys. Res., *103*, 17111–17128, 1998a.
- Kärcher, B.
On the potential importance of sulfur-induced activation of soot particles in nascent
jet aircraft exhaust plumes
Atmos. Res., *46*, 293–305, 1998b.
- Kärcher, B., R. Busen, A. Petzold, F.P. Schröder, U. Schumann, and E.J. Jensen
Physicochemistry of aircraft-generated liquid aerosols, soot, and ice particles, 2,
Comparison with observations and sensitivity studies
J. Geophys. Res., *103*, 17129–17148, 1998.
- Kärcher, B. and S.K. Meilinger
Perturbation of the aerosol layer by aviation-produced aerosols: A parametrization
of plume processes
Geophys. Res. Lett., *25*, 4465–4468, 1998.
- Kärcher, B. and S. Solomon
On the composition and optical extinction of particles in the tropopause region
J. Geophys. Res., *104*, 27441–27460, 1999.
- Kamm, S., O. Möhler, K.-H. Naumann, H. Saathoff, and U. Schurath
The heterogeneous reaction of ozone with soot aerosol
Atmos. Environ., *33*, 4651–4661, 1999.
- Kittelson, D.B.
Engines and nonoparticles: A review
J. Aerosol Sci., *29*, 575–588, 1998.
- Koop, Th., H.P. Ng, L.T. Molina, and M.J. Molina
A new optical technique to study aerosol phase transitions: The nucleation of ice
from H₂SO₄ aerosols
J. Phys. Chem. A *102*, 8924–8931, 1998.
- Lawson, R.P., A.J. Heymsfield, S.M. Aulenchbach, and T.L. Jensen
Shapes, sizes and light scattering properties of ice crystals in cirrus and a persistent
contrail during SUCCESS
Geophys. Res. Lett., *25*, 1331–1334, 1998.
- Lelieveld, J., A. Bregman, H.A. Scheeren, J. Ström, K.S. Carslaw, H. Fischer, P.C.
Siegmond, and F. Arnold
Chlorine activation and ozone destruction in the northern lowermost stratosphere
J. Geophys. Res., *104*, 8201–8213, 1999.
- Liou, K.N., P. Yang, Y. Takano, K. Sassen, T. Charlock, and W. Arnott
On the radiative properties of contrail cirrus
Geophys. Res. Lett., *25*, 1161–1164, 1998.

- Marquart, S.
Atmosphärische Auswirkungen einer mit Wasserstoff betriebenen Luftverkehrsflotte. Diploma Thesis (in German), Techn. Univ. Berlin, 91 pp., October, 1999.
- Marquart, S., R. Sausen, M. Ponater, and V. Grewe
Estimate of the climate impact of cryoplanes
Aerosp. Sci. Technol., submitted, 2000.
- Meilinger, S.K., B. Kärcher, and Th. Peter
Limitation of heterogeneous chemistry on aviation-produced aerosols
Geophys. Res. Lett., 27, in press, 2000.
- Minnis, P., D.F. Young, D.P. Garber, L. Nguyen, W.L. Smith Jr., and R. Palikonda
Transformation of contrails into cirrus during SUCCESS
Geophys. Res. Lett., 25, 1157–1160, 1998.
- Petzold, A., R. Busen, F.P. Schröder, R. Baumann, M. Kuhn, J. Ström, D.E. Hagen, P.D. Whitefield, D. Baumgardner, F. Arnold, S. Borrmann, and U. Schumann
Near-field measurements on contrail properties from fuels with different sulfur content
J. Geophys. Res., 102, 29867–29880, 1997.
- Rogers, D.C., P.J. DeMott, S.M. Kreidenweis, and Y. Chen
Measurements of ice-nucleating aerosols during SUCCESS
Geophys. Res. Lett., 25, 1383–1386, 1998.
- Schmidt, E.
Die Entstehung von Eisnebel aus den Auspuffgasen von Flugmotoren.
Schriften der deutschen Akademie der Luftfahrtforschung, 44, Verlag R. Oldenbourg, München und Berlin, 1–15, 1941.
- Schröder, F.P., B. Kärcher, A. Petzold, R. Baumann, R. Busen, C. Hoell, and U. Schumann
Ultrafine aerosol particles in aircraft plumes: In situ observations
Geophys. Res. Lett., 25, 2789–2792, 1998.
- Schröder, F.P., C.A. Brock, R. Baumann, A. Petzold, R. Busen, P. Schulte, and M. Fiebig
In situ studies on volatile jet exhaust particle emissions – Impacts of fuel sulfur content and thermodynamic conditions on nuclei mode aerosols
J. Geophys. Res., 105, in press, 2000a.
- Schröder, F.P., B. Kärcher, C. Duroure, J. Ström, A. Petzold, J.-F. Gayet, B. Strauss, P. Wendling, and S. Borrmann
The transition of contrails into cirrus clouds
J. Atmos. Sci., 57, 464–480, 2000b.
- Schumann, U.
On conditions for contrail formation from aircraft exhaust
Meteorol. Z. N.F., 5, 4–23, 1996.
- Schumann, U.
Influence of propulsion efficiency on contrail formation
Aerosp. Sci. Technol., submitted, 2000a.

- Schumann, U.
Contrail cirrus
In: D.K. Lynch et al. (Eds.), *Cirrus*, Oxford Univ. Press, in press, 2000b.
- Schumann, U., J. Ström, R. Busen, R. Baumann, K. Gierens, M. Krautstrunk, F.P. Schröder, and J. Stingl
In situ observations of particles in jet aircraft exhausts and contrails for different sulfur containing fuels
J. Geophys. Res., *101*, 6853–6869, 1996.
- SPARC (Stratospheric Processes and Their Role in Climate) – Assessment of Trends in the Vertical Distribution of Ozone
Eds.: N. Harris, R. Hudson, and C. Philips
SPARC Rep. No. 1, WMO Ozone Research and Monitoring Project Rep. No. 43, 289 pp., 1998.
- Ström, J. and S. Ohlsson
In situ measurements of enhanced crystal number densities in cirrus clouds caused by aircraft exhaust
J. Geophys. Res., *103*, 11355–11361, 1998.
- Sussmann, R. and K.M. Gierens
Lidar and numerical studies on the different evolution of vortex pair and secondary wake in young contrails
J. Geophys. Res., *104*, 2131–2142, 1999.
- Twohy, C.H. and B.W. Gandrud
Electron microscope analysis of residual particles from aircraft contrails
Geophys. Res. Lett., *25*, 1359–1362, 1998.
- Weisenstein, D.K., M.K.W. Ko, I.G. Dyominov, G. Pitari, L. Ricciardulli, G. Visconti, and S. Bekki
The effects of sulfur emissions from HSCT A 2D model intercomparison
J. Geophys. Res., *103*, 1527–1547, 1998.
- Yu, F. and R.P. Turco
The role of ions in the formation and evolution of particles in aircraft plumes
Geophys. Res. Lett., *24*, 1927–1930, 1997.
- Yu, F. and R.P. Turco
Contrail formation and impacts on aerosol properties in aircraft plumes: Effects of fuel sulfur content
Geophys. Res. Lett., *25*, 313–316, 1998.
- Yu, F. and R.P. Turco
Evolution of aircraft-generated volatile particles in the far wake regime: Potential contributions to ambient CCN/IN
Geophys. Res. Lett., *25*, 313–316, 1998.
- Yu, F., R.P. Turco, and B. Kärcher
The possible role of organics in the formation and evolution of ultrafine aircraft particles
J. Geophys. Res., *104*, 4079–4087, 1999.